Wind turbine emissions: Interdisciplinary analysis and mitigation approaches – Project Inter-Wind. Description of datasets “Inter-Wind“ and „Inter-Wind (recorder log files)“

Laura Gaßner[1,*] **(laura.gassner@kit.edu), Joachim Ritter**[1] **(joachim.ritter@kit.edu)**
[*] *corresponding author,* [1] *Karlsruhe Institute of Technology (KIT), Geophysical Institute (GPI), Hertzstr. 16, 76187 Karlsruhe, Germany*

Abstract

Within the Inter-Wind project we study wind turbine (WT) emissions with ground motion[1] and acoustic[2] measurements which are accompanied by the acquisition of meteorological parameters[3] as well as psychological surveys[4] of residents living in the vicinity of the wind farms. Measurements are conducted on the Swabian Alb in Southern Germany at wind farms Tegelberg and Lauterstein in multiple interdisciplinary campaigns. Here we focus on measurements with line and ring layouts which are directed at improving the prediction of ground-motion emissions of WTs.

1 Introduction

A significant increase of the overall seismic noise level with increasing wind speed has been found for ground motion recording stations in the vicinity of wind turbines (WTs). The impact of WTs and their emissions on ground motion recording stations as well as residents near wind farms are the subject of several studies in the last few years (e.g., Zieger and Ritter, 2018; Neuffer et al., 2019; Michaud et al., 2016). Discrete frequency peaks can be allocated to the tower vibrations and the blade passing frequency (BPF) of the WT, which is three times the rotation rate, as well as its multiples (Nagel et al., 2021). These frequency peaks appear during time windows with high wind speeds. Although the signal amplitudes are significantly below the threshold of human perception, they can influence the performance of sensitive measuring equipment (Saccorotti et al., 2011; Stammler and Ceranna, 2016; Estrella et al., 2017; Neuffer and Kremers, 2017; Zieger and Ritter, 2018).
The main goals of the Inter-Wind project are the characterization of WT ground motion and acoustic emissions, their correlation with meteorological parameters and the reported annoyance of residents (Gaßner et al., 2022). Furthermore, we aim at the prediction of emissions related to WT operation parameters. The studied wind farms consist of 3 and 16 WTs (Figure 1) of the type GE 2.75-120, respectively, which have a hub height of 139 m, a rotor diameter of 120 m and 2.78 MW rated power. Supervisory-Control-And-Data-Acquisition (SCADA) data are provided by the wind farm operators for the measurement periods, including wind speed, wind direction and rotation rate.
In November 2021, 19 ground motion recording stations have been deployed in a ring and a line layout at wind farm Tegelberg and 13 stations in January 2022 at wind farm Lauterstein. 20 ground motion recording stations (10 MARK 1 s and 10 Trillium Compact 120 s sensors with CUBE3 data loggers) were provided by the GIPP (Geophysical Instrument Pool Potsdam). The instruments were operated for 29 and 40 days, respectively.

[1] Geophysical Institute (GPI), Karlsruhe Institute of Technology (KIT)
[2] Stuttgart Wind Energy (SWE), University of Stuttgart
[3] Zentrum für Sonnenenergie- und Wasserstoffforschung Baden-Württemberg (ZSW), Stuttgart
[4] MSH Medical School Hamburg and Martin-Luther-University Halle-Wittenberg

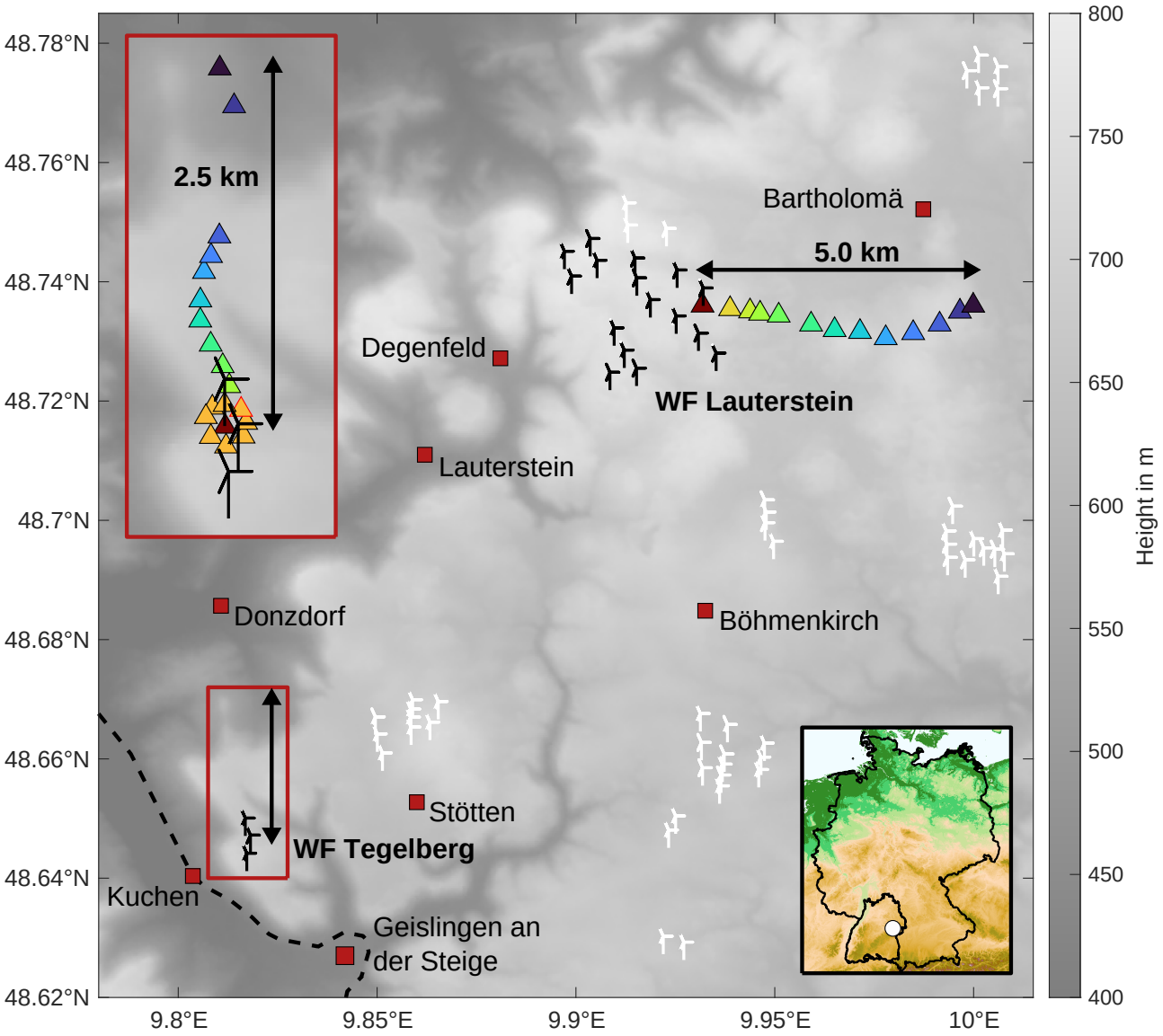

Figure 1: Inter-Wind study area with relevant places and locations of WTs (black - data access for Inter-Wind, white - no data access). Colored triangles show the recording station positions for measurement campaigns at wind farms Tegelberg (inset - top left) and Lauterstein. The dashed line indicates the main railway line Stuttgart-Ulm. Inset (bottom right): map of Germany with the outline of the state of Baden-Württemberg. The white marker denotes the location of the project area.

2 Data acquisition

2.1 Experiment design and schedule

Within the framework of Inter-Wind, we deployed and operated a total of 32 ground-motion recording stations for two time periods of 29 days and 40 days, respectively, at the two wind farms Tegelberg and Lauterstein (Figure 1). The measurements were conducted during the months November 2021 to February 2022 in order to include periods of typically high wind speeds with continuous WT operation. In the first measurement campaign (Table 1) one station (IW05A) was installed on the foundation within the tower of the northernmost WT of wind farm Tegelberg. Eight stations were set up in approximately 150 m distance to this WT at azimuths of 0° (North - IW05I), 45° (Northeast - IW05H), 90° (East - IW05G), 135° (Southeast - IW05F), 180° (South - IW05E), 225° (Southwest - IW05D), 270° (West - IW05C), and 315° (Northwest - IW05B). Ten stations (IW05J-S) were installed up to a distance of approximately 2.5 km to the north of the wind farm. All stations except IW05A (WT), IW05B-C (forest), and IW05Q (backyard of a private property) were deployed and buried on farm land.
As a power supply twenty 9 V block batteries were used for the Trillium Compact instruments along the measurement line and 72 D-cell batteries for the MARK instruments during the ring measurements. The sensors were buried to a depth of about 20-30 cm for insulation and protection of the sensors (Figure 2). The installation took place on 19–23 November 2021 and the stations were removed on 17 December 2021.
A total of 13 seismic stations (IW06A-M, Table 2) were deployed along a linear profile of approximately 5 km length to the west of one of the westernmost WTs of wind farm Lauterstein (Figure 1). Again, one station was installed on the foundation within the WT tower (IW06A). All other instruments were deployed in forest areas except IW06E (on farm land) and IW06F (in a nature reserve). The installation took place on 14 and 21 January 2022 with an additional service trip on 28 January to replace batteries of the MARK instruments. During the installation and service a snow cover of approximately 20 cm was present. The stations were removed on 22 February 2022 after five days of very strong winds (storms Dudley, Eunice and Franklin - German naming: Orkane Ylenia, Zeynep, Antonia).

2.2 Network geometry and location

Tables 1 and 2 list the station names with corresponding locations, elevations, sensor types and data loggers including serial numbers (IDs) as well as runtime periods of the individual instruments.

2.3 Instrumentation

20 sensors (10 MARK L-4C-3D and 10 Trillium Compact) and 20 data loggers (DATA-CUBE3) were kindly provided by the Geophysical Instrument Pool Potsdam (GIPP[5]) for the line and ring measurements, in combination with external battery boxes for the MARK instrument setup. The stations recorded data with three components (vertical, N-S, E-W) and a sampling rate of 100 Hz.
Tables 1 and 2 list the individual instrumentation configurations at each recording site for the two measurement campaigns. We installed ten Trillium Compact (eigenperiod 120 s) and nine MARK (eigenperiod 1 s) instruments at wind farm Tegelberg and seven Trillium Compact and six MARK instruments at wind farm Lauterstein. The gain of the CUBE3 was set to 16 for MARK instruments and to 1 for Trillium Compact instruments. The Trillium Compact instruments were used with breakout boxes (BOB) with a split ratio of 1:10.

[5] https://www.gfz-potsdam.de/en/section/geophysical-imaging/infrastructure/geophysical-instrument-pool-potsdam-gipp/pool-components/seismic-pool

Figure 2: Exemplary instrument installation at recording site IW05H. The sensors and the battery boxes were protected with plastic bags against moisture and the sensors were buried to a depth of about 20 cm (MARK instruments) or 30 cm (Trillium Compact instruments). The Trillium Compact sensors were additionally fixed to the ground with fast-drying cement to ensure stability. Plastic cable protection was used against rodents for all cables. Left: Buried MARK sensor inside a plastic bag. The CUBE3 data logger and the battery box are located at the surface. Right: The site after the installation.

Table 1: Instrumentation information including serial numbers of the used sensors and data loggers for each recording station of measurement campaign IW05 (wind farm Tegelberg). Note that station IW05H failed after 4 days due to a loose power-supply cable.

Station	Location, Altitude	Sensor ID	Logger ID	Runtime
IW05A	48.64704N, 9.81692E, 672 m	MARK-1331	CUBE3-378	2021/11/19 - 2021/12/17
IW05B	48.64826N, 9.81569E, 656 m	MARK-1351	CUBE3-401	2021/11/19 - 2021/12/17
IW05C	48.64766N, 9.81507E, 636 m	MARK-1339A	CUBE3-379	2021/11/19 - 2021/12/17
IW05D	48.64639N, 9.81554E, 679 m	MARK-1333A	CUBE3-377	2021/11/19 - 2021/12/17
IW05E	48.64578N, 9.81700E, 683 m	MARK-289	CUBE3-380	2021/11/19 - 2021/12/17
IW05F	48.64641N, 9.81868E, 673 m	MARK-1356A	CUBE3-449	2021/11/19 - 2021/12/17
IW05G	48.64729N, 9.81893E, 666 m	MARK-1346A	CUBE3-381	2021/11/19 - 2021/12/17
IW05H	48.64812N, 9.81844E, 660 m	MARK-1340	CUBE3-382	2021/11/19 - 2021/11/23
IW05I	48.64843N, 9.81686E, 662 m	MARK-1333	CUBE3-383	2021/11/19 - 2021/12/17
IW05J	48.64963N, 9.81731E, 663 m	TC-170	CUBE3-448	2021/11/22 - 2021/12/17
IW05K	48.65091N, 9.81668E, 667 m	TC-172	CUBE3-414	2021/11/22 - 2021/12/17
IW05L	48.65228N, 9.81553E, 670 m	TC-167	CUBE3-423	2021/11/22 - 2021/12/17
IW05M	48.65382N, 9.81453E, 676 m	TC-168	CUBE3-446	2021/11/22 - 2021/12/17
IW05N	48.65510N, 9.81454E, 674 m	TC-174	CUBE3-416	2021/11/22 - 2021/12/17
IW05O	48.65692N, 9.81489E, 671 m	TC-173	CUBE3-418	2021/11/22 - 2021/12/17
IW05P	48.65794N, 9.81556E, 674 m	TC-176	CUBE3-447	2021/11/22 - 2021/12/17
IW05Q	48.65919N, 9.81636E, 691 m	TC-178	CUBE3-417	2021/11/22 - 2021/12/17
IW05R	48.66750N, 9.81777E, 503 m	TC-169	CUBE3-422	2021/11/23 - 2021/12/17
IW05S	48.66991N, 9.81640E, 513 m	TC-175	CUBE3-415	2021/11/23 - 2021/12/17

Table 2: Instrumentation information including serial numbers of the used sensors and data loggers for each recording station of measurement campaign IW06 (wind farm Lauterstein). Note that there are data gaps for all Mark sensors (except IW06M) up to 2022/01/28 because of battery failure due to low temperatures.

Station	Location, Altitude	Sensor ID	Logger ID	Runtime
IW06A	48.73603N, 9.93184E, 746 m	TC-168	CUBE3-448	2022/01/14 - 2022/02/22
IW06B	48.73543N, 9.93877E, 743 m	TC-175	CUBE3-414	2022/01/21 - 2022/02/22
IW06C	48.73505N, 9.94378E, 689 m	MARK-289	CUBE3-450	2022/01/21 - 2022/02/22
IW06D	48.73467N, 9.94631E, 683 m	TC-169	CUBE3-418	2022/01/21 - 2022/02/22
IW06E	48.73435N, 9.95099E, 670 m	MARK-1331	CUBE3-379	2022/01/14 - 2022/02/22
IW06F	48.73284N, 9.95913E, 667 m	TC-176	CUBE3-417	2022/01/21 - 2022/02/22
IW06G	48.73192N, 9.96505E, 720 m	MARK-1340	CUBE3-449	2022/01/14 - 2022/02/22
IW06H	48.73161N, 9.97143E, 726 m	TC-172	CUBE3-422	2022/01/14 - 2022/02/22
IW06I	48.73056N, 9.97790E, 719 m	MARK-1333	CUBE3-383	2022/01/14 - 2022/02/22
IW06J	48.73141N, 9.98481E, 713 m	TC-167	CUBE3-416	2022/01/14 - 2022/02/22
IW06K	48.73284N, 9.99145E, 710 m	MARK-1339A	CUBE3-378	2022/01/14 - 2022/02/22
IW06L	48.73501N, 9.99656E, 704 m	TC-170	CUBE3-446	2022/01/14 - 2022/02/22
IW06M	48.73601N, 9.99990E, 659 m	MARK-1333A	CUBE3-401	2022/01/21 - 2022/02/22

Table 3: Properties of the used sensors and data loggers. The CUBE3 data loggers were set to gain 16 for the MARK instrument and to gain 1 for the Trillium Compact instruments. For the Trillium Compact additionally BOBs with a split ratio of 1:10 were used.

Sensor	A/D conversion in counts/V	Sensitivity in V/(m/s)	Norm. factor	Poles		Zeros
MARK L-4C-3D	6.5536e7	170	1.0	-4.443	+4.443i	0
				-4.443	-4.443i	0
Trillium Compact	4.096e5	754.3	4.34493e17	-0.03691	+0.03702i	0
				-0.03691	-0.03702i	0
				-343		-392
				-370	+467i	-1960
				-370	-467i	-1490 +1740i
				-836	+1522i	-1490 -1740i
				-836	-1522i	
				-4900	+4700i	
				-4900	-4700i	
				-6900		
				-15000		

Logger and sensor characteristics[6] to deconvolve time series to true ground motion velocity from the raw data are listed in Table 3. Instrument response functions for the used sensors based on the values of Table 3 are displayed in Figure 3.

3 Data quality and accuracy

All instruments were installed using a gyro compass to ensure an accurate orientation towards north with an accuracy of approximately $\pm 0.3°$. GPS reception for time synchronisation was fine for all stations during both measurement campaings and all stations contribute to the full data set in combination with cycled GPS recordings. The only exception is station IW05H which failed four days after installation because of a loose power-supply cable. Due to low temperatures and battery failure there are data gaps of several days for stations IW06C, IW06E, IW06G, IW06I, and IW06K up to 28 February 2022.

Figures 4 and 5 show record sections for earthquakes in Peru with magnitudes of Mw=7.5 and Mw=6.5, respectively, for the vertical components. The seismic data is bandpass filtered between 0.1–5 Hz and the amplitudes are scaled to a constant factor for each plot. The distance of each station is relative to the location of the one WT of each wind farm where an instrument was installed on the foundation (sites IW05A and IW06A). All stations recorded a clear onset of the earthquake P-phase. The signal-to-noise ratio (SNR) is very similar at all sites. Data from the stations inside the WT towers are not shown as their amplitudes during WT operation are much larger than the earthquake signals.

The power spectral densities (PSD) of each component for all ground motion stations outside the WT towers are shown in Figures 6 and 7. In each figure, data from one day with no or moderate WT operation are shown alongside data from days with full wind farm operation with respect to the New Low Noise Model (NLNM) and the New High Noise Model (NHNM) after Peterson (1993).

Signal levels are increased at IW05Q above 1 Hz and at IW05S above 10 Hz, due to significant anthropogenic noise. Furthermore, it can be observed that the horizontal components show significantly lower signal levels below 10 Hz and an increased signal level above at sites IW05B, IW06C, IW06K, and IW06M (all Mark instruments) compared to the other stations. This can also be seen in day-spectrograms for the respective data, where low frequencies seem to fade out gradually and independently on each component (Figures 8-10). We suspect a gradual tilting of the instruments to be responsible for this behaviour which affects the horizontal components only. Potentially, thawing of the ground and/or insufficient stability of the buried instruments in the forest ground could be reasons for the tilting.

4 Data availability and access

The data are archived in the GFZ Seismological Data Archive (GEOFON) with the network code 4C (2020-2024) where it will be made freely available to the scientific community in April 2023. The data sets can be accessed via http://geofon.gfz-potsdam.de/waveform/. Recommended citation is: Gaßner, L., Ritter, J. (2022) Inter-Wind. GFZ Data Services. Other/Seismic Network. https://doi.org/10.14470/9P982225.

The recorder log files with the GPS information are archived at the GIPP Experiment and Data Archive and can be requested via GFZ Data Services (https://dataservices.gfz-potsdam.de). Recommended citation for this log file dataset is: Gaßner, L., Ritter, J. (2023) Inter-Wind (recorder log files). GFZ Data Services. https://doi.org/10.5880/GIPP.202125.1.

[6] https://www.gfz-potsdam.de/en/section/geophysical-imaging/infrastructure/geophysical-instrument-pool-potsdam-gipp/pool-components/poles-and-zeros

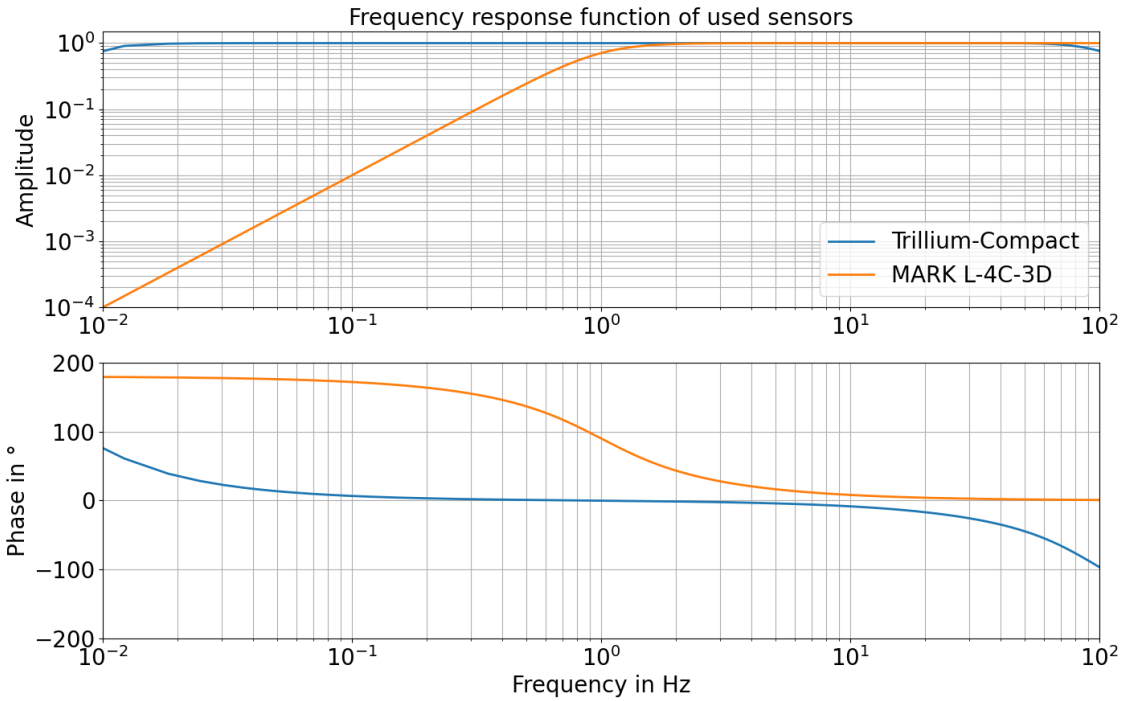

Figure 3: Instrument response functions of the two used sensors Trillium Compact and MARK L-4D-3C, computed with the values given in Table 3.

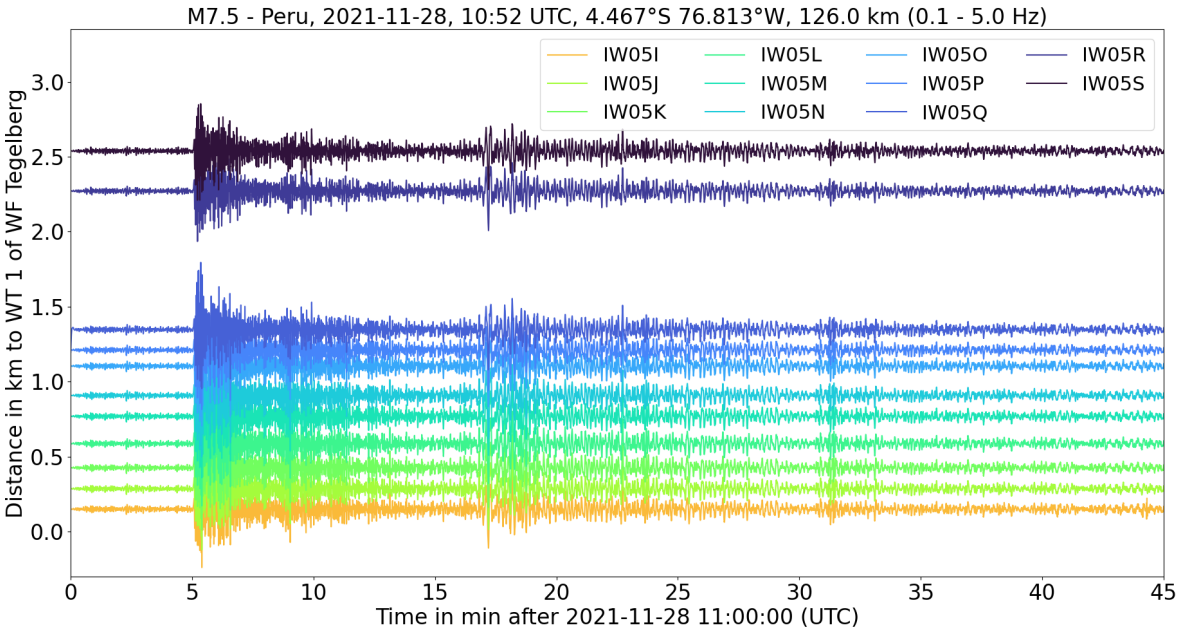

Figure 4: Record section of vertical component data from campaign IW05 for an earthquake with a magnitude of Mw=7.5 in Peru. The distance of each station is relative to WT 1 of WF Tegelberg. From the ring measurement only station IW05I is shown for clarity. The seismic data is bandpass filtered between 0.1-5 Hz.

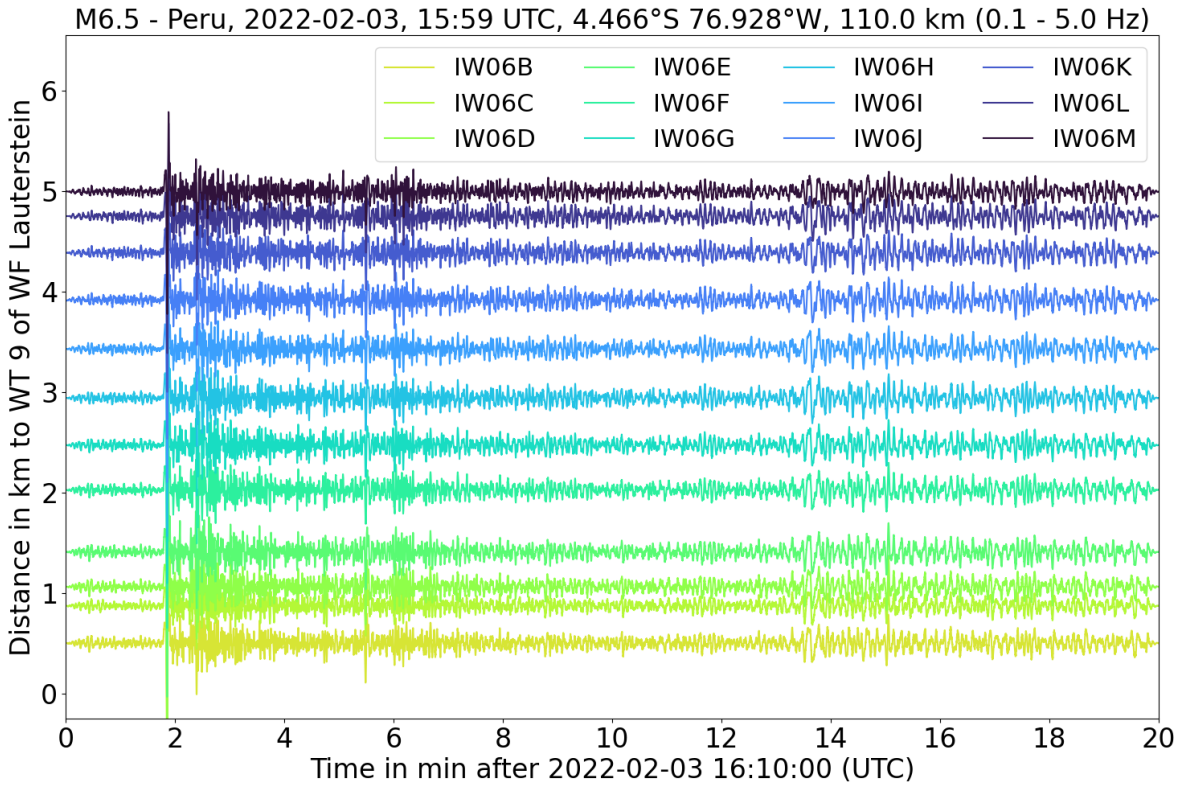

Figure 5: Record section of vertical component data from campaign IW06 for an earthquake with a magnitude of Mw=6.5 in Peru. The distance of each station is relative to WT 9 of WF Lauterstein. The seismic data is bandpass filtered between 0.1-5 Hz.

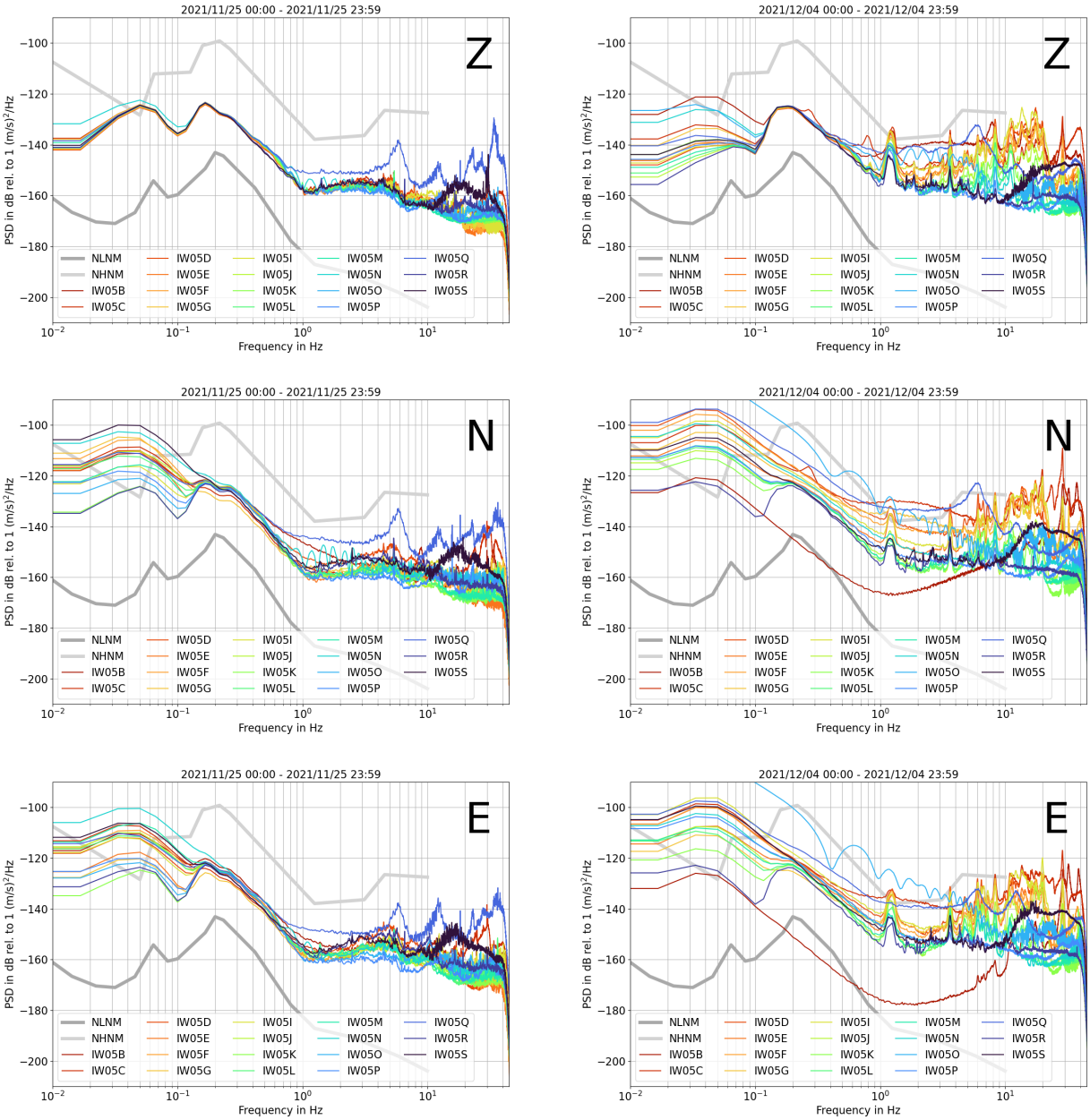

Figure 6: PSDs of all stations of campaing IW05 (except IW05A) at wind farm Tegelberg with the NLNM and NHNM (Peterson, 1993) indicated as gray lines. Left: 2021/11/25 with no WT operation, right: 2021/12/04 with full wind farm operation. Z, N, E: vertical, north-south, and east-west components.

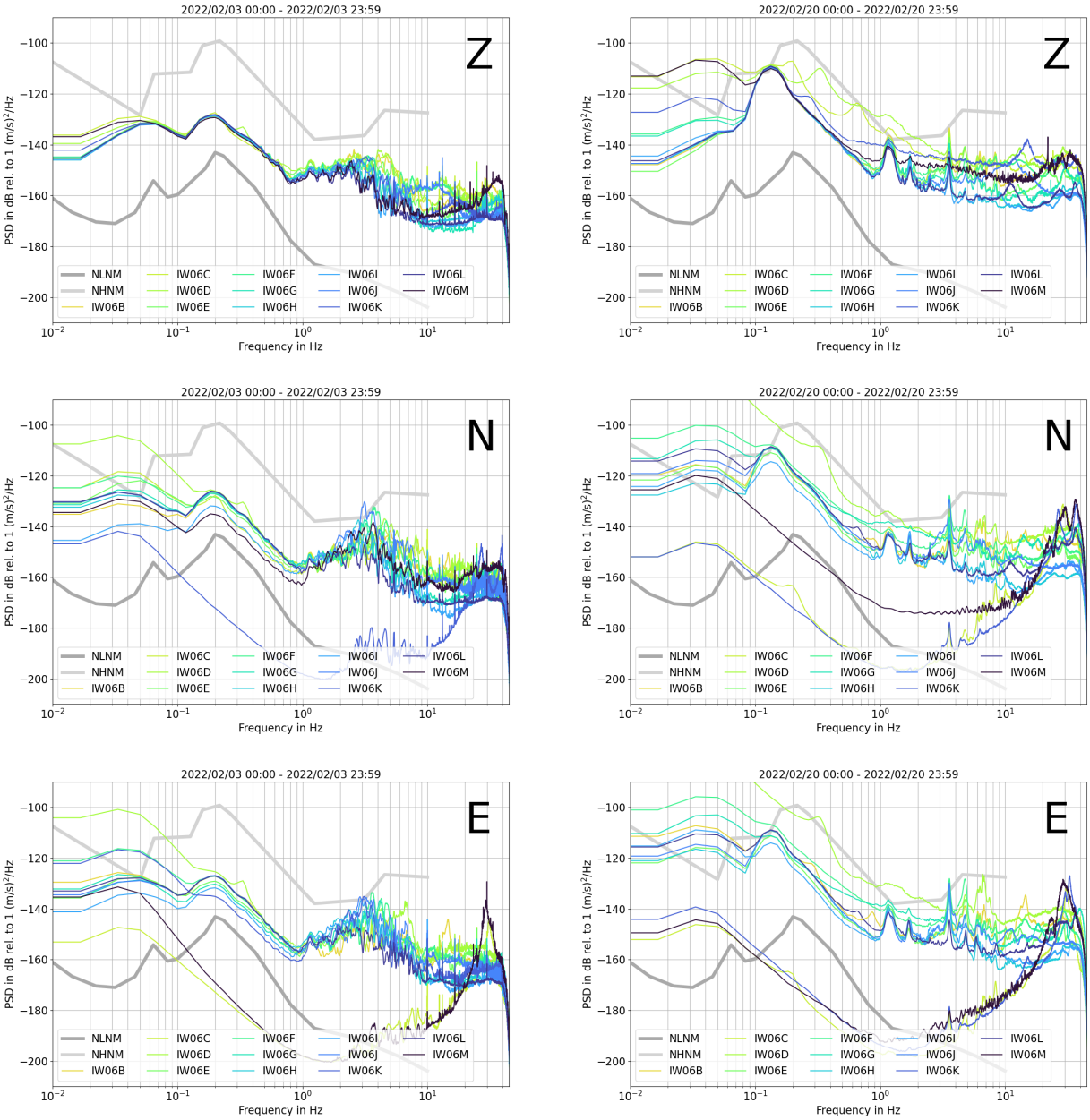

Figure 7: PSDs of all stations of campaing IW06 (except IW06A) at wind farm Lauterstein with the NLNM and NHNM (Peterson, 1993) indicated as gray lines. Left: 2022/02/03 with moderate WT operation, right: 2022/02/20 with full wind farm operation. Z, N, E: vertical, north-south, and east-west components.

Acknowledgements

We thank the local authorities of the municipalities Donzdorf and Bartholomä for their support. We also thank the Stadtwerke Schwäbisch Hall and the KWA Contracting AG for providing access to WT 1 and the WT operating data at wind farm Tegelberg, as well as the wpd windmanager technik GmbH for access and data related to wind farm Lauterstein. We acknowledge the support of local residents, Forst BW and the Regierungspräsidium Stuttgart (department 56) that allowed the installation of instruments on their property. Felix Bögelspacher, Leon Merkel, Marie Gärtner, Rune Helk, Ankitha Pezhery, and Amelie Nüsse helped with the installation and maintenance of the ground motion sensors. This study is supported by the Federal Ministry for Economic Affairs and Climate Action based on a resolution of the German Bundestag (grant 03EE2023D).

References

Estrella, H. F., Korn, M., and Alberts, K. (2017). Analysis of the influence of wind turbine noise on seismic recordings at two wind parks in Germany. Journal of Geoscience and Environment Protection, 5(5):76–91. https://doi.org/10.4236/gep.2017.55006

Gaßner, L., Blumendeller, E., Müller, F. J. Y., Wigger, M., Rettenmeier, A., Cheng, P. W., Hübner, G., Ritter, J., and Pohl, J. (2022). Joint analysis of resident complaints, meteorological, acoustic, and ground motion data to establish a robust annoyance evaluation of wind turbine emissions. Renewable Energy, 188:1072–1093. https://doi.org/10.1016/j.renene.2022.02.081

Michaud, D. S., Feder, K., Keith, S. E., Voicescu, S. A., Marro, L., Than, J., Guay, M., Denning, A., McGuire, D., Bower, T., et al. (2016). Exposure to wind turbine noise: Perceptual responses and reported health effects. The Journal of the Acoustical Society of America, 139(3):1443–1454. https://doi.org/10.1121/1.4942391

Nagel, S., Zieger, T., Luhmann, B., Knödel, P., Ritter, J., and Ummenhofer, T. (2021). Ground motions induced by wind turbines. Civil Engineering Design, 3:73–86. https://doi.org/10.1002/cend.202100015

Neuffer, T. and Kremers, S. (2017). How wind turbines affect the performance of seismic monitoring stations and networks. Geophysical Journal International, 211(3):1319–1327. https://doi.org/10.1093/gji/ggx370

Neuffer, T., Kremers, S., and Fritschen, R. (2019). Characterization of seismic signals induced by the operation of wind turbines in North Rhine-Westphalia (NRW), Germany. Journal of Seismology, 23(5):1161–1177. https://doi.org/10.1007/s10950-019-09866-7

Peterson, J. R. (1993). Observations and modeling of seismic background noise. Technical report, US Geological Survey. https://doi.org/10.3133/ofr93322

Saccorotti, G., Piccinini, D., Cauchie, L., and Fiori, I. (2011). Seismic noise by wind farms: a case study from the Virgo Gravitational Wave Observatory, Italy. Bulletin of the Seismological Society of America, 101(2):568–578. https://doi.org/10.1785/0120100203

Stammler, K. and Ceranna, L. (2016). Influence of wind turbines on seismic records of the Gräfenberg array. Seismological Research Letters, 87(5):1075–1081. https://doi.org/10.1785/0220160049

Zieger, T. and Ritter, J. R. (2018). Influence of wind turbines on seismic stations in the upper rhine graben, SW Germany. Journal of Seismology, 22(1):105–122. https://doi.org/10.1007/s10950-017-9694-9

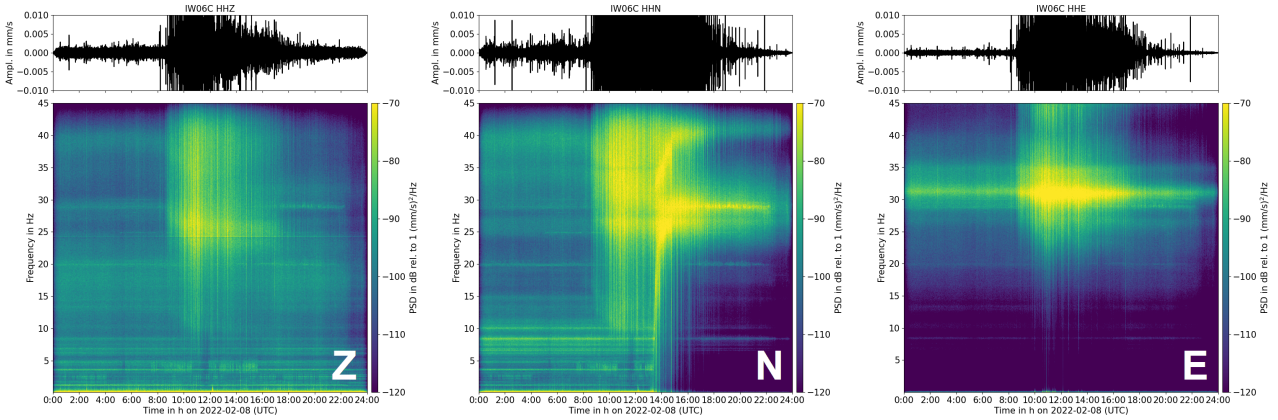

Figure 8: Spectrograms for site IW06C on 2022/02/08 showing the effect of tilting on the N-component (left: Z-component, middle: N-component, right: E-component).

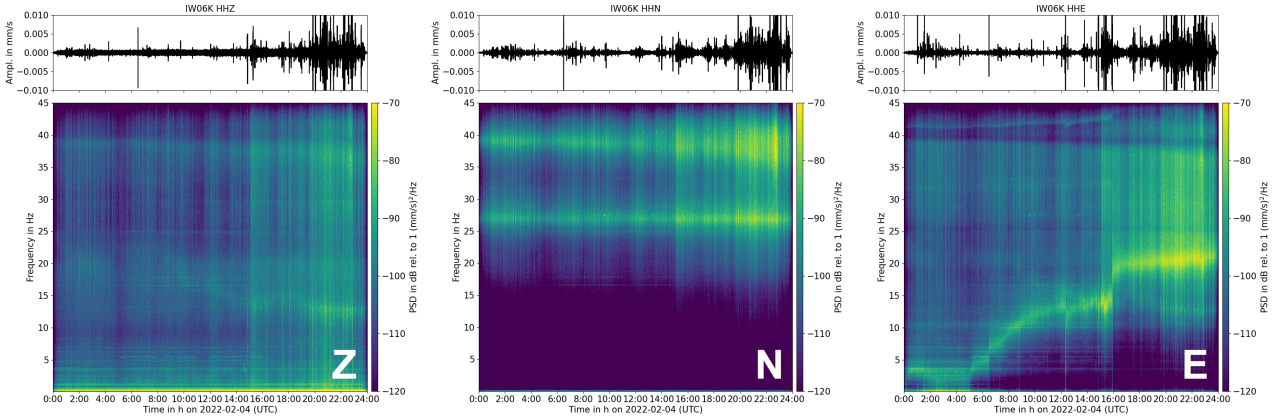

Figure 9: Spectrograms for site IW06K on 2022/02/04 showing the effect of tilting on the E-component (left: Z-component, middle: N-component, right: E-component).

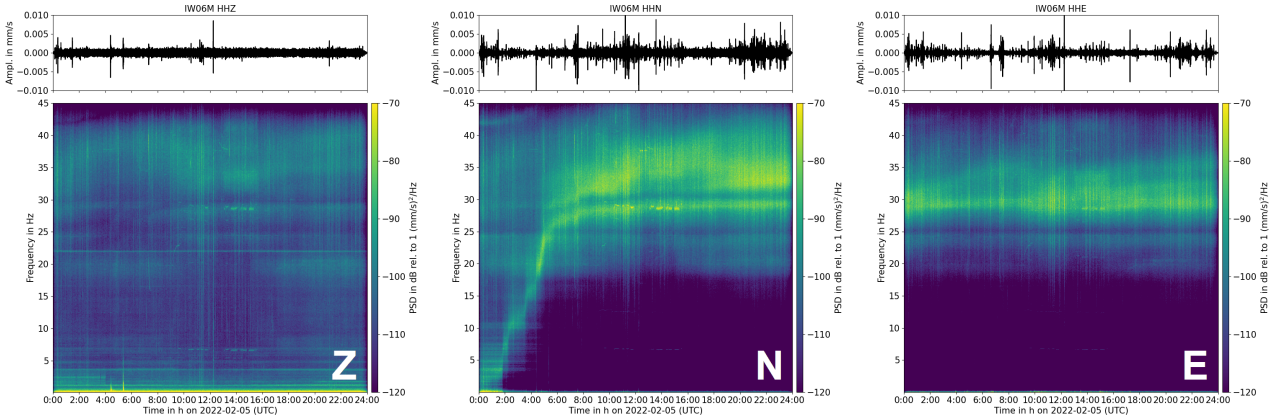

Figure 10: Spectrograms for site IW06M on 2022/02/05 showing the effect of tilting on the N-component (left: Z-component, middle: N-component, right: E-component).